Environ. Sci. Technol. **2005**, *39,* 6616−6623

Changes in Zinc Speciation in Field Soil after Contamination with Zinc Oxide

ANDREAS VOEGELIN,*,† SABINA PFISTER,† ANDREAS C. SCHEINOST,‡ MATTHEW A. MARCUS,§ AND RUBEN KRETZSCHMAR†

Institute of Terrestrial Ecology, Swiss Federal Institute of Technology (ETH) Zurich, Switzerland, Institute of Radiochemistry, Forschungszentrum Rossendorf (FZR), Dresden, Germany, and Advanced Light Source, Lawrence Berkeley National Laboratory, Berkeley, California 94720

Recent studies on the speciation of Zn in contaminated soils confirmed the formation of Zn-layered double hydroxide (LDH) and Zn−phyllosilicate phases. However, no information on the kinetics of the formation of those phases under field conditions is currently available. In the present study, the transformation of Zn in a field soil artificially contaminated with ZnO containing filter dust from a brass foundry was monitored during 4 years using extended X-ray absorption fine structure (EXAFS) spectroscopy. Soil sections were studied by μ-X-ray fluorescence (μ-XRF) and μ-EXAFS spectroscopy. EXAFS spectra were analyzed by principal component analysis (PCA) and linear combination fitting (LCF). The results show that ZnO dissolved within 9 months and that half of the total Zn reprecipitated. The precipitate was mainly of the Zn−LDH type (>75%). Only a minor fraction (<25%) may be of Zn−phyllosilicate type. The remaining Zn was adsorbed to soil organic and inorganic particles. No significant changes in Zn speciation occurred from 9 to 47 months after the contamination. Thermodynamic calculations show that both Zn−LDH and Zn−phyllosilicate may form in the presence of ZnO but that the formation of Zn−phyllosilicate would be thermodynamically favored. Thus, the dominance of Zn−LDH found by spectroscopy suggests that the formation of the Zn precipitates was not solely controlled by thermodynamics but also contained a kinetic component. The rate-limiting step could be the supply of Al and Si from soil minerals to the Zn-rich solutions around dissolving ZnO grains.

Introduction

Zinc is an essential element for all organisms, and Zn deficiency is a widespread problem in agriculture and human nutrition. On the other hand, soils may become contaminated with Zn from mining, smelting, and other industrial activities, from the runoff of galvanized steel constructions, or from road runoff. Zinc may then reduce the soil microbial activity and cause phytotoxic effects. This may lead to reduced crop yields in agriculture or to a reduced plant cover and land degradation in heavily affected areas. The bioavailability and mobility of Zn in soils are to a large degree determined by its chemical speciation. The adsorption of Zn to various soil components such as organic matter, clay minerals, and Fe and Mn (hydr)oxides has been studied extensively in the past decades. State-of-the-art multisurface adsorption models for Zn in soils account for Zn adsorption to all these individual surfaces (*1*). However, recent studies on Zn sorption to pure minerals have shown that the incorporation of Zn in newly forming mineral phases may also represent a relevant sequestration pathway in soils and sediments. Depending on the nature of the mineral surface and the kinetics of the supply of Al and Si from the weathering of primary minerals, the resulting phases were shown to be of the layered double hydroxide (LDH), phyllosilicate, or hydroxide type (*2*−*5*). The formation of Zn−LDH was also observed in laboratory studies using soil (*6*). Studies on the speciation of Zn in soils that were heavily contaminated from smelter emissions confirmed the formation of Zn−phyllosilicate as well as Zn−LDH phases under field conditions (*7*, *8*). Both Zn−LDH and Zn−phyllosilicate are layered phases containing Zn in octahedral sheets (Figure 1). Substitution of Zn by Al in the trioctahedral sheets of Zn−LDH gives rise to a net positive charge, which is compensated by anions in the interlayers (not shown in Figure 1). In the phyllosilicate structure, tetrahedral Si-sheets are attached to either one side of the trioctahedral sheet (Figure 1, 1:1 clay minerals) or to both sides (not shown, 2:1 clay minerals). Other layered Zn phases detected in recent years include Zn incorporated into the gibbsite-like dioctahedral sheets of Al-hydroxy interlayered clay minerals (HIM) in acidic soils (*9*) and of the Mn mineral lithiophorite (*10*, *11*). The common characteristic of all those species is the incorporation of Zn into the octahedral sheets of layered minerals. To date, the knowledge about the quantitative significance of precipitate formation for Zn speciation and about the kinetics of precipitate formation under field conditions is still limited.

In the present study, the speciation of Zn in a field soil artificially contaminated with ZnO containing filter dust from a brass foundry was monitored during 4 years using bulk extended X-ray absorption fine structure (EXAFS) spectroscopy on powder samples and μ-X-ray fluorescence (μ-XRF) and μ-EXAFS spectroscopy on soil sections. The objectives were (i) to follow the transformation of Zn upon contamination with time, (ii) to determine the type of precipitates forming, and (iii) to derive the kinetics and quantitative relevance of their formation.

Experimental Procedures

Field Lysimeter. The present study was conducted within an interdisciplinary project addressing the influence of heavy metal contamination (Zn, Cd, Cu, Pb) in a soil on ecosystem functioning from the level of single cells to whole organisms (Cell-Tree project). For this purpose, open-top lysimeters were filled with calcareous subsoil and freshly excavated topsoil material. The topsoil material had developed from fluvioglacial deposits. It was noncalcareous, had a loamy texture (360 g/kg sand, 490 g/kg silt, 150 g/kg clay), a mixed clay mineralogy (kaolinite, mica, chlorite, vermiculite, hydroxy-interlayered vermiculite), and contained 15 g/kg organic C. The soil had a pH of 6.5 (measured in 10 mM $CaCl_2$), and the effective cation exchange capacity (CEC) was 55 $mmol_c$/kg. The topsoil material contained 99 mg/kg Zn, 837 mg/kg Mn, and 19380 mg/kg Fe. After emplacement of the soil, the contamination was introduced by manually

* Corresponding author phone: ++41 44 633 61 47; fax: ++41 44 633 11 18; e-mail: voegelin@env.ethz.ch.
† Swiss Federal Institute of Technology.
‡ Forschungszentrum Rossendorf.
§ Lawrence Berkeley National Laboratory.

10.1021/es047962g CCC: $30.25

Published on Web 07/30/2005

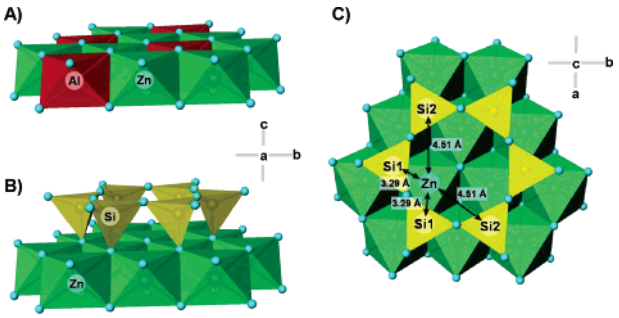

FIGURE 1. (A) Structure of the octahedral sheet of Zn-LDH containing Zn and Al atoms in a ratio of 2 to 1. Side view along *a*-axis. (B) Structure of Zn−phyllosilicate with tetrahedral Si sheet attached to the octahedral Zn sheet (example for lizardite-type 1:1 phyllosilicate). Sideview along *a*-axis. (C) Top view on Zn−phyllosilicate structure along *c*-axis indicating the positions of nearest (Si1 at 3.29 Å) and next nearest (Si2 at 4.51 Å) Si atoms around Zn.

mixing filter dust from a brass foundry into the first 20 cm of the topsoil. The filter dust contained about 654 g/kg Zn, 65 g/kg Cu, 12 g/kg Pb, and 0.3 g/kg Cd. It consisted of about 850 g/kg zincite (ZnO), 100 g/kg brass (approximate composition $Cu_{0.6}Zn_{0.4}$), and minor amounts (<10 g/kg) of other Zn minerals. After contamination, the average initial metal concentrations in the topsoil were 2800 mg/kg Zn, 410 mg/kg Cu, 100 mg/kg Pb, and 10 mg/kg Cd. During 4 years, the soil remained in the planted lysimeters. The field site was located at the Swiss Federal Institute for Forest, Snow, and Landscape (WSL) at 550 m above sea level. The local climate is moderate with a mean annual temperature of 8.5 °C and 1100 mm of annual rainfall.

Soil Sampling. Bulk soil samples of 50−500 g were collected directly after mixing the filter dust into the soil (0 months) and at increasing intervals after the contamination (2, 4, 9, 19, 20, 36, 37, 47, and 48 months) in the same field lysimeter. The samples were dried at 60 °C and sieved to <2 mm. The soil samples contained between 2300 and 3900 mg/kg Zn. The Zn concentrations did not systematically decrease with time but were reflecting the heterogeneous mixing of the filter dust into the topsoil material. Preliminary results from pore water analysis and soil extracts suggest that Zn leaching into the calcareous subsoil was not significant within the experimental 4 years period (personal communication, Jörg Luster, WSL, 2005). For bulk EXAFS analysis, the soil was ball-milled to <50 μm. Samples for the preparation of soil sections were collected 18 and 36 months after contamination. After 18 months, undisturbed soil was collected in Kubiena boxes (8 cm × 6 cm × 5 cm). After 36 months, soil cores of about 4 cm length and 2.5 cm diameter were extracted in aluminum tubes. The samples were frozen and freeze-dried. They were then embedded with LR White resin in a vacuum and heated to 60 °C for hardening. Sections of 500 μm thickness were cut using a diamond cutting wheel and subsequently ground and polished.

Bulk EXAFS Analysis. Bulk-EXAFS spectra of the soil samples and references were collected at the Zn K-edge. For those analyses, we used the beamline X11A at the National Synchrotron Light Source (NSLS, Brookhaven), the ANKA-XAS beamline at the Angströmquelle Karlsruhe (ANKA, Karlsruhe, Germany), and the Rossendorf Beamline (ROBL) and the Swiss Norwegian Beamline (SNBL) at the European Synchrotron Radiation Facility (ESRF, Grenoble, France). All spectra were collected at room temperature. The raw data were transformed into *k*-space using the WinXAS software (*12*). The pre- and postedge background correction was performed by fitting a first- and second-order polynomial function, respectively. The E_0 was determined as the inflection point of the Zn K-edge (second derivative equal to zero). The μ_0 was fit using a cubic spline function and minimizing the amplitude of the Fourier transform at radial distances (*r*) less than 0.9 Å. Fourier transforms were calculated using a Kaiser−Bessel window (window parameter $a = 4$).

μ-XRF and μ-EXAFS Analysis. Element mapping and microspectroscopic analyses were performed at the beamline 10.3.2 at the Advanced Light Source (ALS, Berkeley, CA) (*13*). The soil sections were mounted in a 45° angle to the incident beam, and the fluorescence signal was recorded in a 90° angle using a Ge seven-element solid-state detector. Element mapping was carried out at 10 keV incident photon energy using a beam size of 5 × 5 μm^2. Zn K-edge EXAFS spectra at selected points were recorded using the same beam size. The χ-spectra were extracted as described for the bulk EXAFS spectra.

Reference Spectra. A total of 65 reference spectra for Zn in mineral structures, Zn adsorbed to mineral surfaces, and Zn complexed by organic substances was compiled from our own as well as published spectra. It included, among others, zincite (ZnO, Merck), Zn−orthophosphate ($Zn_3(PO_4)_2$, Alfa Aesar), Zn−Al−LDH (*6*), Zn in Al−hydroxy interlayered montmorillonite (*9*), Zn−phyllosilicate (synthesized according to the method described in ref *14*), Zn bearing birnessite at high coverage (*15*), Zn bearing birnessite at low coverage (*16*), Zn adsorbed to ferrihydrite (*15*), Zn adsorbed to montmorillonite (pH 5.7, 48 000 mg/kg adsorbed Zn, 32 mM Zn in solution), Zn adsorbed to purified humic acid (pH 6, 350 mg/kg Zn), Zn−malate and Zn−phytate (*17*), and aqueous Zn. The spectra for Zn−birnessite at high coverage and Zn−ferrihydrite were kindly provided by Donald L. Sparks (University of Delaware), and the spectrum of Zn−phytate was provided by Alain Manceau (CNRS, Université Joseph Fourier, France).

Data Analysis. For data interpretation, principal component analysis (PCA), target transform testing (TT), and linear combination fitting (LCF) were carried out using SixPack (Samuel Webb, Stanford Synchrotron Radiation Laboratory) and the programs from the ALS beamline 10.3.2. On the basis of the k^3-weighted χ-spectra of the bulk- and micro-EXAFS measurements (*k*-range from 2 to 10 $Å^{-1}$, interpolated to 0.05*k* grid), PCA analysis in combination with TT provides the basis to define the number and types of reference spectra suitable for subsequent LCF analysis of the experimental EXAFS spectra. LCF analyses were carried out by first adding the reference spectrum giving the lowest sum of squared residuals ($SSR = \Sigma_i(k^3\chi_{exp} - k^3\chi_{fit})^2$). The next reference spectrum added was the one giving the largest decrease in SSR. If the decrease in SSR was less than 10%, further references were not considered.

Results and Discussion

Bulk EXAFS Spectra. Figure 2A shows bulk EXAFS spectra of the soil collected immediately after the soil had been contaminated (0 months) and at increasing incubation times (2, 4, 9, and 47 months). Reference spectra are depicted in Figure 3. The initial bulk soil spectrum (0 months) closely resembles the spectrum of ZnO, reflecting the major component of the filter dust mixed into the soil. Also, the spectrum after 2 months is still dominated by the spectral contribution of ZnO. Between months 2 and 4 after contamination, the bulk soil spectrum changes dramatically, and only minor features such as the peak at 6.5 $Å^{-1}$ and the rise of the signal above 9 $Å^{-1}$ still indicate contributions from ZnO after 4 months. In the spectrum collected after 9 months, also those features have disappeared, indicating that most ZnO had been dissolved by that time. Only minor changes in the bulk soil spectrum are observed between 9 and 47 months. The small splitting observed in the peak at 3.5 $Å^{-1}$ as well as the shape of the spectrum above 7 $Å^{-1}$ resembles the reference

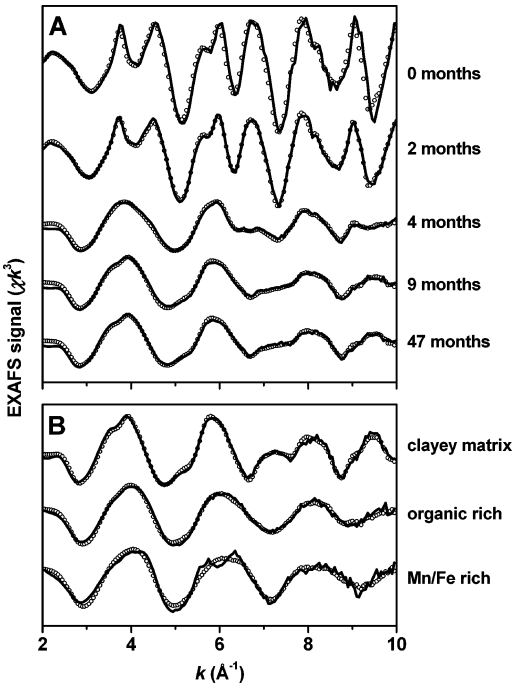

FIGURE 2. Zn K-edge EXAFS spectra from (A) bulk soil samples collected at increasing incubation times and (B) from characteristic zones in soil sections (solid lines). Linear combination fits using reference spectra for ZnO, Zn−LDH, Zn−phytate, and aqueous Zn (dots, LCF results in Table 4).

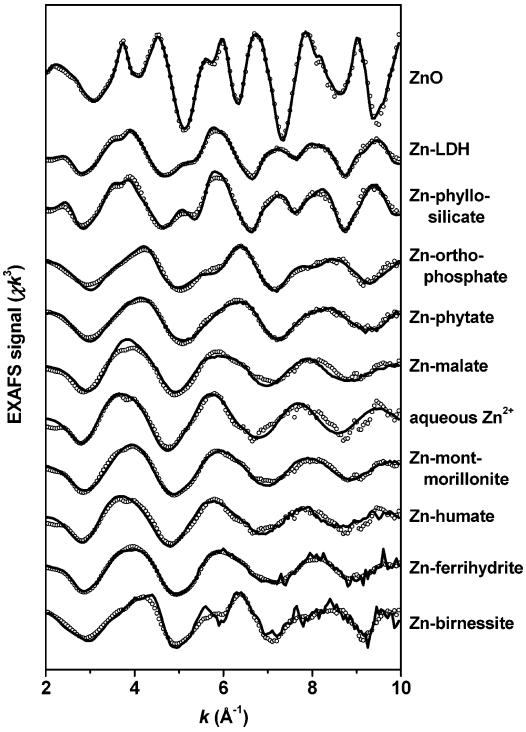

FIGURE 3. Zn K-edge EXAFS spectra for selected reference compounds (solid lines) and target transforms (dots, Table 3) using the first four components obtained from the principal component analysis (Table 2).

spectra for Zn−LDH or Zn−phyllosilicate, indicating that a layered precipitate may have formed in the soil.

Element Mapping and μ-EXAFS Analysis. To better delineate the types of Zn species that had formed in the soil upon ZnO dissolution, we studied the Zn distribution and speciation on soil sections taken after 18 and 36 months

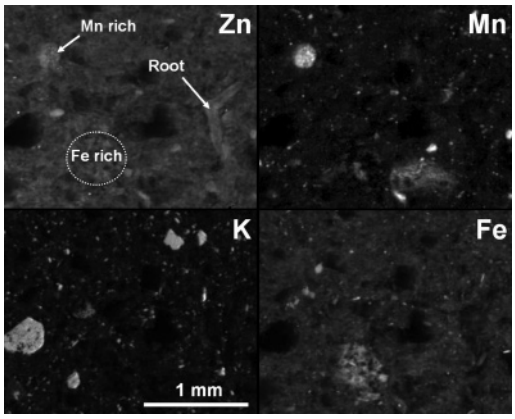

FIGURE 4. μ-XRF maps for Zn, Mn, K, and Fe (intensities in regions of interest). Zn occurs diffusely distributed in the clayey soil matrix, associated with Mn and Fe rich zones and with organic structures such as roots. Area is 2.4 × 2 mm².

using μ-XRF and μ-EXAFS spectroscopy. Figure 4 shows the distribution (uncalibrated intensities within regions of interest) of Zn, Mn, K, and Fe on a 2.4 mm × 2 mm area of a soil section collected after 36 months. The maps demonstrate the complexity of the soil fabric, with Mn and Fe enriched zones, organic debris, and a fine-grained clay matrix. On the basis of the results of element mapping, a total of 26 μ-EXAFS spectra was collected on selected spots from soil sections collected after 18 and 36 months. Morphologically, the spots at which most spectra were taken could be assigned to one of three distinct groups. Those three groups of spectra were clearly related to the three typical soil environments mentioned before: the fine-grained clayey soil matrix, Mn/Fe rich zones, and organic rich zones. Representative μ-EXAFS spectra for each of these zones are depicted in Figure 2B. The similarity between the spectrum from the clayey soil matrix and the bulk EXAFS spectra collected after 9 and 47 months indicates that the Zn diffusely distributed in the clayey soil matrix accounts for most of the Zn in the soil. This spectrum bears also considerable similarity with the reference spectrum of Zn−LDH (Figure 3). The spectrum measured on an organic rich spot compares to the spectrum of Zn−phytate, which was shown to be a suitable reference for Zn sorbed to plant roots (*17*). The spectrum from the Mn/Fe rich zones exhibits a split at 6 $Å^{-1}$. This splitting occurs also in the spectrum of Zn sorbed to birnessite at low surface coverage (Figure 3, reference spectrum from ref *16*), suggesting that this Zn species might be present in the Mn/Fe rich spots. In contrast to the spectrum from the clayey soil matrix, the spectra from the organic rich and Mn/Fe rich region show less resemblance with the bulk EXAFS spectrum from the soil after 47 months (Figure 2), suggesting that they account for a smaller fraction of the total Zn. A linear combination fit of this bulk spectrum with the μ-EXAFS spectra gave 64.1% contribution from the clay matrix and 29.2% from the organic rich spectrum (Figure 5A and Table 1). The addition of the Mn/Fe rich μ-EXAFS spectrum only leads to an insignificant improvement in the LCF (64.6% clayey matrix, 26.6% organic rich, 2.1% Mn/Fe rich, SSR 17.2, NSS 2.1%, fit not shown). This result confirms that Zn in the clayey matrix represents most of the total Zn, that a smaller fraction is associated with organic materials, and that only a minor fraction is associated with Mn/Fe rich zones. The good match of the fit suggests that the μ-EXAFS spectra contain all relevant Zn species present in the soil.

PCA-TT Analysis. The visual inspection of the bulk- and μ-EXAFS spectra already gave indications as to which reference spectra might be suitable for LCF analysis (ZnO, Zn−LDH, Zn−phytate, Zn−birnessite). Taking advantage of the information contained in all experimental spectra, a

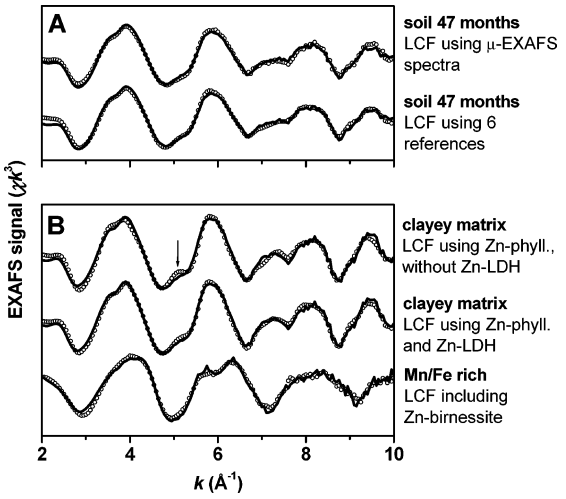

FIGURE 5. (A) LCF of the bulk soil spectrum after 47 months using the μ-EXAFS spectra from Figure 2 or using an extended set of references that includes Zn−phyllosilicate and Zn−birnessite. (B) LCF of the μ-EXAFS spectrum from the clayey matrix using either the spectrum of Zn−phyllosilicate or the spectra of Zn−phyllosilicate and Zn−LDH as proxies for the soil formed precipitate and LCF of the μ-EXAFS spectrum from the Mn/Fe rich spot including the spectrum of Zn−birnessite. The arrow indicates a deviation in the LCF caused by the use of the Zn−phyllosilicate reference spectrum. LCF parameters are provided in Table 1.

principal component analysis was next run on the total of 10 bulk and 26 μ-EXAFS spectra. PCA provides an orthogonal set of components describing the whole suite of experimental spectra, whereby the components are ranked by decreasing relevance (*18*, *19*). The parameters of the first eight components obtained by PCA are given in Table 2. The indicator function IND provides a means to determine the number of relevant components and should be minimal for the number of relevant components. This was the case for four components, suggesting four major spectral contributions in our experimental spectra. However, the minimum of the IND function is not very pronounced, and only 70% of the total experimental variance could be described by the first four components. This might indicate that more than four Zn species contribute to the experimental signal, some of them having similar spectra. The first four components would then account for the main features of those species, while further details are only covered by additional components. This interpretation is supported by the results of a PCA run on the 11 reference spectra shown in Figure 3, which gave the lowest IND for four components (explaining 84% of the total variance). Therefore, we used the first four and six components from the PCA for target transformation (i.e., to test reference spectra for their suitability to describe the experimental data). This was done using the SPOIL value of each reference spectrum obtained by TT. Depending on their SPOIL value, reference spectra can be classified as excellent (SPOIL < 1.5), good (1.5−3), acceptable (3−4.5), poor (4.5−6), or unacceptable (SPOIL > 6) (*18*, *19*). Results for selected reference spectra are provided in Table 3. Not surprisingly, the contaminant phase ZnO with its distinct EXAFS spectrum was most clearly identified as a reference phase by TT. Target testing also returned a low SPOIL for Zn−LDH, while the SPOIL of Zn−phyllosilicate was higher both with four and six components. This suggests that a precipitate of predominantly LDH-type contributes to the spectra but does not allow excluding the presence of Zn−phyllosilicate. If Zn−LDH and Zn−phyllosilicate always occur together in similar relative amounts, PCA would not identify the individual spectra but only their mixture. Therefore, TT was also performed on calculated mixtures of Zn−LDH and Zn−phyllosilicate (from 95% Zn−LDH/5% Zn−phyllosilicate to 5% Zn−LDH/95% Zn−phyllosilicate in 5% steps). The lowest SPOIL with four components (2.19) was obtained for the spectrum of 75% Zn−LDH and 25% Zn−phyllosilicate. This result suggests that predominantly Zn−LDH and a minor fraction of Zn−phyllosilicate occur intimately associated in the clayey soil matrix and cannot be resolved as single species using μ-EXAFS. However, because the reference spectra of Zn−LDH and Zn−phyllosilicate are similar, the approach may not be sensitive to the true speciation, and the results may simply represent the optimal fit of the calculated spectrum to the SPOIL criterion. On the basis of these considerations, the Zn−LDH spectrum was used as the reference for subsequent LCF since it seems to represent the predominant fraction of the precipitate that had formed in the soil. With ZnO and Zn−LDH, two reference spectra were chosen to account for the initial contaminant phase and a neoformed Zn−precipitate. On the basis of the PCA results, at least two more reference spectra were required to describe the experimental spectra. Adsorbed Zn may occur both in tetrahedral and in octahedral coordination on organic and inorganic substrates, depending on the type of sorbent and on surface coverage (*16*, *20*−*23*). On the basis of the aforementioned consideration that PCA mainly indicates the main spectral features common to various species, it was therefore expected that the two remaining spectra would basically represent tetrahedrally and octahedrally coordinated adsorbed Zn. From the Zn reference spectra shown in Figure 3, Zn−orthophosphate, Zn−phytate, Zn−malate, Zn−birnessite, and Zn−ferrihydrite contain mainly tetrahedrally coordinated Zn, while Zn−humate, Zn−montmorillonite, and aqueous Zn represent species with octahedrally coordinated Zn. For these spectra, by far the lowest SPOIL values (using both four and six components) were obtained for Zn−phytate (tetrahedrally coordinated Zn) and aqueous Zn (octahedrally coordinated). Therefore, Zn−phytate was chosen as the reference spectrum for tetrahedrally coordinated adsorbed Zn and aqueous Zn as the reference spectrum for octahedrally coordinated adsorbed Zn. In terms of chemistry, it should be noticed that tetrahedrally coordinated Zn will always be inner spherically adsorbed, while octahedrally coordinated Zn may occur both as an inner sphere as well as an outer sphere sorption complex. To summarize, based on PCA, four reference spectra were selected for subsequent LCF: ZnO as the initial contaminant phase, Zn−LDH representing the neoformed Zn−precipitate phase, and Zn−phytate and aqueous Zn representing tetrahedrally and octahedrally coordinated adsorbed Zn, respectively.

LCF on Bulk-EXAFS Spectra. The LCF for the bulk- and μ-EXAFS spectra using the four reference spectra selected by PCA are shown in Figure 2, and fit parameters are provided in Table 4. The LCF results for the bulk spectra show that the ZnO dissolved within 9 months and that half of the total Zn was incorporated into a newly formed precipitate phase of mostly Zn−LDH type. These fits were based on the criterion that only spectra causing SSR to decrease by more than 10% were considered. If all species contributing more than 1% to the fitted spectrum were used, 2−4% ZnO could also be fit in spectra collected after 9, 19, and 20 months but not in those collected after 37, 47, and 48 months. This suggests that the complete dissolution of all ZnO took somewhat longer than 9 months. However, the major fraction of ZnO had been dissolved after 9 months, and only minor changes in Zn speciation subsequently occurred up to 47 months (Table 4). The spectrum of the soil collected after 47 months was fit as a combination of 55% Zn−LDH, 34% Zn−phytate, and 17% aqueous Zn. Thus, about half of the total Zn in the soil was sequestered into a precipitate of mostly Zn−LDH type, about one-third was present as a tetrahedral inner sphere

TABLE 1. Parameters of the Linear Combination Fits Presented in Figure 5

	LCF of the bulk soil spectrum after 47 months based on the μ-EXAFS spectra from Figure 2					
	clayey matrix (%)	organic rich (%)	Mn/Fe rich (%)	sum (%)	SSR (%)[a]	NSSR (%)[b]
soil 47 months	64.1	29.2		93.3	17.2	2.1

	LCF of the bulk soil spectrum after 47 months and of the μ-EXAFS spectra using two additional reference spectra							
	Zn−LDH (%)	Zn−phyll. (%)[c]	aq. Zn^{2+} (%)[d]	Zn−phytate (%)	Zn−birnes. (%)[e]	sum (%)	SSR (%)[a]	NSSR (%)[b]
soil 47 months	37.0	14.1	18.2	29.7	4.8	103.8	19.0	2.3
clayey matrix		56.4	27.8	22.8		107.0	34.6	3.1
clayey matrix	60.0	17.7	14.4	21.5		113.5	21.6	1.9
Mn/Fe rich			20.1	51.1	28.7	99.9	35.2	4.2

[a] SSR (sum of squared residuals) = $\Sigma_i((k^3\chi_{exp} - k^3\chi_{fit})^2)$. [b] NSSR (normalized sum of squared residuals) = $\Sigma_i((k^3\chi_{exp} - \chi_{fit})^2)/\Sigma_i((k^3\chi_{exp})^2)$. [c] Zn−phyllosilicate. [d] Aqueous Zn. [e] Zn−birnessite.

TABLE 2. Results from the Principal Component Analysis on 10 Bulk and 26 μ-EXAFS Spectra

component	eigenvalue	variance	cum. var.[a]	IND	TNSSR[b]
1	168.3	0.392	0.392	0.0126	22.8
2	73.0	0.170	0.562	0.0082	8.3
3	46.9	0.109	0.671	0.0047	2.3
4	13.2	0.030	0.701	0.0045	1.9
5	8.7	0.020	0.722	0.0046	1.7
6	8.4	0.019	0.741	0.0047	1.5
7	7.8	0.018	0.759	0.0048	1.3
8	7.4	0.017	0.776	0.0049	1.1

[a] Cumulative variance. [b] $TNSSR = \Sigma_{spectra}(\Sigma_i((k^{3*}\chi_{exp} - k^{3*}\chi_{fit})^2))/\Sigma_{spectra}(\Sigma_i((k^{3*}\chi_{exp})^2))$.

TABLE 3. Spoil Values of Reference Spectra Obtained by Target Transformation Using the First Four and Six Components[a]

	SPOIL		
reference	$N = 4$	$N = 6$	LCF[b]
ZnO	1.54	1.01	X
Zn−LDH	2.50	1.64	X
Zn−phyllosilicate	3.00	2.80	(x)
Zn−orthophosphate	3.06	3.21	
Zn−phytate	2.02	2.24	X
Zn−malate	5.09	3.45	
aqueous Zn	2.00	1.89	X
Zn sorbed montmorillonite	3.62	2.83	
Zn−humate	2.64	2.51	
Zn sorbed ferrihydrite	6.63	6.33	
Zn sorbed birnessite (low coverage)	6.13	4.29	(x)

[a] The target transforms with four components are displayed in Figure 3. [b] Spectra marked with an X were used for the LCF calculations shown in Figure 2. Spectra marked with an (x) were added for the LCFs shown in Figure 5.

sorption complex, and about one-sixth as octahedral Zn, either in inner sphere or in outer sphere sorption mode.

LCF of the μ-EXAFS Spectrum from the Clayey Soil Matrix. The LCF of the μ-EXAFS spectrum from the clayey soil matrix yields a predominant contribution of 83.9% from the Zn−LDH reference spectrum (Figure 2 and Table 4). The Fourier transforms (FT) of the experimental spectrum and the LCF are shown in Figure 6 (spectrum a). The LCF matches the experimental data closely within the *r*-range of 0.5−6.5 Å, with respect to both the amplitude and the imaginary part of the FT. If the Zn−phyllosilicate instead of the Zn−LDH reference spectrum was used as a proxy for the neoformed Zn precipitate, the LCF deteriorated both in *k*- as well as in *r*-space (Figure 5B, Figure 6, and Table 1). This finding is in agreement with the better match of the TT of the Zn−LDH than the Zn−phyllosilicate reference spectrum (Figure 3) and the higher SPOIL of the Zn−phyllosilicate reference spectrum (Table 3). In *r*-space, the LCF with the Zn−phyllosilicate reference exhibits a mismatch between 3.4 and 4.5 Å (Figure 6). The peak observed in the LCF results from the contribution of the Zn−phyllosilicate spectrum and is related to the backscattering of second nearest Si atoms at ∼4.5 Å from the central atom in the Zn−phyllosilicate structures (*2*, *24*). The location of the second nearest Si neighbors is exemplified in Figure 1 for a lizardite-like Zn−phyllosilicate. The Zn−LDH does not contain a tetrahedral Si sheet attached to the octahedral sheet and yields a good match of LCF and experimental data in the *r*-range of 0.5−6.5 Å. In agreement with the PCA-TT approach, these structural considerations further corroborate that the Zn precipitate in the soil was predominantly of the Zn−LDH type. If both the Zn−LDH and the Zn−phyllosilicate spectrum were used in the LCF, the fit did not greatly improve as compared to the LCF with only Zn−LDH (Figures 5B and 6). The decrease of SSR by approximately 10% may simply be caused by the addition of an additional reference (Tables 1 and 4). Considering the Fourier transform plot, the addition of the Zn−phyllosilicate reference may also allow us to obtain a slightly better fit of the first and second shell peaks without providing a clearly improved fit in the *r*-range of 3.4−4.5 Å. The sum of the fitted fractions of Zn−LDH and Zn−phyllosilicate (77.7%) was similar to the fraction of Zn−LDH (83.9%) in the LCF with only Zn−LDH (Tables 1 and 4). The ratio of Zn−LDH and Zn−phyllosilicate in the LCF of approximately 3:1 was close to the ratio of the calculated mixed reference spectrum giving the lowest SPOIL in PCA-TT. Considering that the LCF in *k*- and *r*-space did not clearly improve and that the fraction of Zn−phyllosilicate fitted in other μ-EXAFS spectra from the clayey matrix was always lower than in the spectrum discussed here, the LCF suggests that the precipitate phase was predominantly of the Zn−LDH type and that at most, 25% of the precipitate was of the Zn−phyllosilicate type.

LCF on μ-EXAFS Spectra from Organic and Mn/Fe Rich Areas. The spectrum of the organic rich zone (root debris) was fit with 68.7% Zn−phytate, 24.9% Zn−LDH, and 12.5 aqueous Zn (Table 4). This result compares well to the findings of Sarret et al. (*17*), who showed in a hydroponic study with *Arabidopsis halleri* that Zn bound to phosphate groups represents a major Zn species on plant roots. The spectrum from a Mn/Fe rich spot of the soil section, namely, the split at 6 $Å^{-1}$, could not be reproduced using the selected four references (see LCF in Figure 2). Also, the TT using the four first components did not reproduce that feature, whereas the first six components did (not shown). This splitting is indicative of the presence of Zn sorbed to birnessite at low surface coverage (Figure 3, reference spectrum from ref *16*). By adding this spectrum to the LCF, a substantially improved fit of the μ-EXAFS spectrum also reproducing the observed splitting was achieved with 28.7% Zn−birnessite, 51.1% Zn−

TABLE 4. Results from the Linear Combination Fitting of the Bulk Zn K-Edge EXAFS Spectra Using the Reference Spectra from ZnO, Zn−LDH, Zn−Phytate, and Aqueous Zn^{2+}[a]

	ZnO (%)	Zn−LDH (%)	Zn−phytate (%)	aq. Zn^{2+} (%)	sum (%)	SSR (%)	NSSR (%)
			Bulk spectra				
0 months	90.0				90.0	321.6	8.4
2 months	69.3		16.7	14.8	100.8	18.8	0.7
4 months	13.8	41.4	31.6	17.7	104.5	18.8	2.3
9 months		50.8	37.2	18.6	106.6	20.0	2.4
47 months		55.0	33.7	16.6	105.4	20.5	2.5
			Micro spectra				
clayey matrix		83.9	21.0	10.8	115.7	24.0	2.1
organic rich		24.9	68.7	12.5	106.1	20.9	2.6
Mn/Fe rich			77.1	23.5	100.6	61.9	7.3

[a] The LCF spectra are displayed in Figure 2.

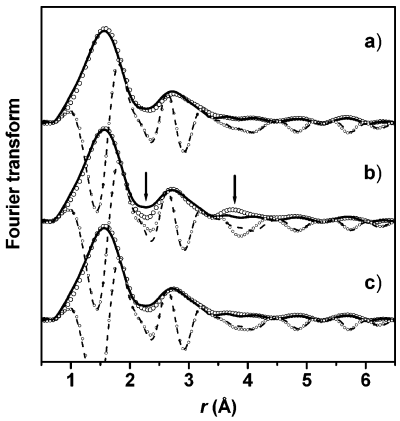

FIGURE 6. Amplitude and imaginary part of the Fourier transform of the μ-EXAFS spectrum from the clayey matrix (solid and dashed lines, respectively). Comparison to LCF curves (open dots) obtained using either Zn−LDH (spectrum a), Zn−phyllosilicate (spectrum b), or Zn−LDH and Zn−phyllosilicate (spectrum c) as proxies for the Zn precipitate. Arrows indicate deviations in spectrum b caused by the use of the Zn−phyllosilicate reference spectrum.

phytate, and 21.1% aqueous Zn (Figure 5B and Table 1). The sum of the fitted fractions of Zn−birnessite and Zn−phytate (79.8%) was close to the fraction of Zn−phytate that was obtained when fitting without the Zn−birnessite reference (77.1%, Table 4). This shows that when Zn−birnessite (and other sorbed species containing Zn in tetrahedral coordination) was not considered explicitly, the Zn−phytate spectrum represented all tetrahedrally coordinated adsorbed Zn in the LCF.

Extended LCF of the Bulk Soil Spectrum after 47 Months. The LCF of the μ-EXAFS spectra suggest that small fractions of Zn−birnessite and Zn−phyllosilicate may be present in the bulk soil. For the spectrum of the bulk soil collected after 47 months, LCF was therefore repeated considering these two additional species (Figure 5A and Table 1). Note that since ZnO is not present anymore after 47 months, the fit was essentially based on five references. The results show that the addition of both Zn−phyllosilicate and Zn−birnessite to the LFC only insignificantly reduced the SSR (Tables 1 and 4). The fitted curve was hardly distinguishable from the one using four references (effectively three without ZnO, Figure 2). On the other hand, the fit results were consistent with the findings from the LCF of the μ-EXAFS spectra: the addition of Zn−phyllosilicate lead to a corresponding reduction in the Zn−LDH fraction without strongly affecting the total fitted amount of Zn precipitates. The contribution of Zn−phyllosilicate to the sum of the precipitates was 28%, in close agreement with the findings from LCF on the μ-EXAFS spectrum of the clayey matrix and the PCA results for calculated mixed reference spectra. As for the μ-EXAFS spectrum from the Mn/Fe rich spot, the addition of Zn−birnessite to the LCF caused a corresponding decrease in the fitted fraction of Zn−phytate. The spectrum of Zn adsorbed to ferrihydrite in tetrahedral coordination exhibits a second shell contribution from Zn/Fe at a distance of about 3.38−3.50 Å (*25*). This is similar to second shell Zn−Mn distances of 3.35−3.50 Å found for Zn sorbed to birnessite (*16*). In Zn−phytate, Zn is coordinated with P at a distance of 3.08 Å in its second shell (*17*). The spectrum of Zn adsorbed to ferrihydrite is therefore expected to be more similar to the spectrum of Zn−birnessite than the spectrum of Zn−phytate. Thus, when adding the spectrum of Zn−birnessite to the LCF, the fitted Zn−birnessite fraction likely also includes Zn adsorbed to ferrihydrite, and the fitted Zn−phytate fraction is expected to mostly represent tetrahedral Zn sorbed to organic substrates. On the basis of these considerations, the following conclusions with respect to the speciation of Zn in the bulk soil after 47 months may be drawn: about half of the Zn is present in a Zn precipitate, which predominantly consists of Zn−LDH (>75%) and may contain a minor fraction of Zn−phyllosilicate (<25%). The other half of the total Zn is mainly present as tetrahedrally coordinated Zn adsorbed to organic sorbents (30% of total Zn) and 18% of octahedrally coordinated Zn, either as an inner or an outer sphere sorption complex. The contribution of tetrahedral Zn sorbed to Mn and Fe (hydr)oxide phases is likely less than 5−10%.

Thermodynamic Considerations on the Formation of Zn−LDH and Zn−Phyllosilicate. In the current study, we find evidence for the predominant formation of Zn−LDH and at most a minor amount of Zn−phyllosilicate in contaminated soil under field conditions. Earlier studies using EXAFS spectroscopy have demonstrated the presence of Zn−LDH (*8*) or Zn−phyllosilicate (*7*) in field soils contaminated from smelter emissions. On the basis of laboratory studies on Zn and Ni sorption to pyrophyllite, Ford et al. (*4*, *30*) showed that initially forming LDH phases are stabilized by silicate in their interlayers. To discuss the formation of Zn−LDH in our soil, we calculated the pore water composition and solubility indices (SI) of Zn−LDH and Zn−phyllosilicate in equilibrium with dissolving ZnO grains in the presence of amorphous $Al(OH)_3$ and soil SiO_2 at atmospheric CO_2 partial pressure (Table 5). The pH of the solution was fixed to 7.0, and the concentration of chloride was fixed at 1 mM, a typical value reported for soil solutions (*27*, *28*). Because the studied soil is relatively young (<10 000 years) and only weakly weathered, amorphous $Al(OH)_3$ and soil SiO_2 were assumed to control the concentrations of Al and Si in the soil solution, respectively. Under these conditions, the solution is highly oversaturated with respect to Zn−phyllosilicate. It is also oversaturated by more than 1 order of magnitude with respect to Zn−LDH containing bicarbonate in the interlayer, while it is undersaturated with respect to Zn−LDH with Cl in the interlayer, even though the calculated CO_3^{2-} concentration

TABLE 5. Calculation of Saturation Indices (SI) for Two Zn−LDH Phases with CO_3^{2-} and Cl^- in the Interlayer and for Zn−Phyllosilicate in Equilibrium with Zincite, Amorphous $Al(OH)_3$, Soil SiO_2, 1 mM Dissolved Cl^-,[a] and Atmospheric CO_2 Partial Pressure (3.2×10^{-4} atm) at pH 7.0

phase	reaction	log K[b]	SI
	Input		
zincite (ZnO)	$ZnO + H_2O \rightleftarrows Zn^{2+} + 2OH^-$	−16.84	0
amorphous $Al(OH)_3$	$Al(OH)_3 \rightleftarrows Al^{3+} + 3OH^-$	−32.34	0
soil SiO_2	$SiO_2 + 2H_2O \rightleftarrows H_4SiO_4$	−3.10	0
	$CO_2(g) + H_2O \rightleftarrows 2H^+ + CO_3^{2-}$	−18.15	
	Output[c]		
Zn−LDH−CO_3	$Zn_2Al(OH)_6(CO_3)_{0.5} \rightleftarrows 2Zn^{2+} + Al^{3+} + 6OH^- + 0.5CO_3^{2-}$	−64.06[d]	1.22
Zn−LDH−Cl	$Zn_2Al(OH)_6Cl \rightleftarrows 2Zn^{2+} + Al^{3+} + 6OH^- + Cl^-$	−60.5[e]	−1.52
Zn−phyllosilicate	$Zn_3Si_4O_{10}(OH)_2 + 10H_2O \rightleftarrows 3Zn^{2+} + 4H_4SiO_4 + 6OH^-$	−76[f]	13.1

[a] Concentration of Cl fixed at typical value for soil solutions (*27*, *28*). [b] Calculations performed without activity correction using constants from ref *26* for zincite, amorphous $Al(OH)_3$, soil SiO_2, and carbonate equilibrium. [c] Equilibrium concentrations in solution: $(Zn^{2+}) = 1.5 \times 10^{-3}$ M, $(CO_3^{2-}) = 2.3 \times 10^{-8}$ M, $(Al^{3+}) = 4.6 \times 10^{-12}$ M, $(H_4SiO_4) = 7.9 \times 10^{-4}$ M. [d] Ref *29*. [e] Ref *4*. [f] Ref *7*.

is several orders of magnitude lower than the Cl concentration. This result was obtained with solubility products from two independent studies (*4*, *29*, *31*) and is in agreement with the expected influence of the interlayer anions on LDH stability (*32*). If the pH was fixed to lower or higher values, the SI of the Zn−LDH−CO_3 and Zn−phyllosilicate remained the same, while the SI of the Zn−LDH−Cl increased with decreasing pH and became positive at pH < 5.5. With respect to the SI of the Zn−LDH−CO_3, the assumption of atmospheric CO_2 partial pressure was rather conservative. Because of soil respiration, CO_2 partial pressures in soil are often higher by about a factor 10, and waterlogging may even result in CO_2 partial pressured that are 100 up to 1000 times higher than the atmospheric pCO_2 (*26*). Thus, soil respiration and waterlogging are factors that strongly favor the formation of Zn−LDH−CO_3. Regarding Zn−phyllosilicate, the H_4SiO_4 concentration calculated in equilibrium with soil SiO_2 is within the range of typical H_4SiO_4 concentrations found in soil solutions of moderately weathered soils (*27*, *28*). Even if the solubility of Si was limited by quartz, resulting in an almost 10 times lower Si concentration, the SI of Zn−phyllosilicate would still equal 9.5. In conclusion, the calculated SI values suggest that the formation of both Zn−LDH and Zn−phyllosilicate is thermodynamically possible. However, the formation of Zn−phyllosilicate is thermodynamically favored over the formation of Zn−LDH, as was pointed out by Manceau et al. (*7*). Under field conditions, though, the dissolution of the ZnO grains and subsequent reprecipitation of Zn is expected to cause depletion of Si and Al in the surrounding pore water. The ratio of the formation of Zn−LDH and Zn−phyllosilicate is then controlled by the supply of Si and Al from the dissolution of primary and secondary soil minerals. In the soil studied in this work, it appears that the availability of Al and Si favors the formation of Zn−LDH. In the long term, however, the thermodynamic data would suggest that Zn−LDH would be transformed into Zn−phyllosilicate.

Environmental Implications. The present study demonstrates the rapid dissolution of ZnO and the rapid formation of a Zn precipitate in a near neutral noncalcareous soil upon contamination with brass foundry emissions. The Zn precipitate is mainly of the LDH-type but may also contain a small phyllosilicate-type fraction (<25%). After 9 months, the Zn precipitate accounts for about half of the total Zn, highlighting the relevance of precipitate phases for an understanding of the impact and fate of Zn in polluted soils. While Zn−phyllosilicate is thermodynamically more stable, kinetic factors seem to favor the initial formation of a Zn−LDH phase in this soil. If such types of precipitates are to be considered in fate and risk assessment models, both kinetic as well as thermodynamic aspects need to be taken into account.

Acknowledgments

We thank Madeleine Goerg-Günthardt and Jörg Luster from the Swiss Federal Institute of Forest, Snow, and Landscape (WSL) for providing soil samples from the Cell-to-Tree project. Kurt Barmettler is acknowledged for technical support in the laboratory. Alain Manceau (Grenoble, France) and Donald L. Sparks (Newark, DE) kindly provided the EXAFS spectra of Zn−phytate and Zn−ferrihydrite, respectively. We thank Kumi Pandya from the beamline X11A at NSLS, Stephan Mangold from the XAS beamline at ANKA (Germany), and the staff from the ROBL and SNBL beamlines at ESRF (France) for their support with bulk EXAFS measurements. The ANKA (Germany) and SNBL and ROBL at the ESRF (France) are acknowledged for the provision of beamtime for bulk EXAFS analyses. The ALS (Berkeley, CA) is acknowledged for providing beamtime at the microfocused beamline 10.3.2. The ALS is supported by the Director, Office of Science, Office of Basic Energy Sciences, Materials Sciences Division of the U.S. Department of Energy under Contract DE-AC03-76SF00098 at the Lawrence Berkeley National Laboratory.

Note Added after ASAP Publication

In Table 5 one of the values in the log K column was incorrect in the version published July 30, 2005. The corrected version was published August 15, 2005.

Literature Cited

(1) Weng, L. P.; Temminghoff, E. J. M.; van Riemsdijk, W. H. Contribution of individual sorbents to the control of heavy metal activity in sandy soil. *Environ. Sci. Technol.* **2001**, *35*, 4436−4443.

(2) Schlegel, M. L.; Manceau, A.; Charlet, L.; Chateignier, D.; Hazeman, J. Sorption of metal ions on clay minerals III. Nucleation and epitaxial growth of Zn phyllosilicates on the edges of hectorite. *Geochim. Cosmochim. Acta* **2001**, *65*, 4155−4170.

(3) Schlegel, M. L.; Manceau, A.; Charlet, L.; Hazeman, J. Adsorption mechanisms of Zn on hectorite as a function of time, pH, and ionic strength. *Am. J. Sci.* **2001**, *301*, 798−830.

(4) Ford, R. G.; Sparks, D. L. The nature of Zn precipitates formed in the presence of pyrophyllite. *Environ. Sci. Technol.* **2000**, *34*, 2479−2483.

(5) Nachtegaal, M.; Sparks, D. L. Effect of iron oxide coatings on zinc sorption mechanisms at the clay-mineral/water interface. *J. Colloid Interface Sci.* **2004**, *276*, 13−23.

(6) Voegelin, A.; Scheinost, A. C.; Bühlmann, K.; Barmettler, K.; Kretzschmar, R. Slow formation and dissolution of Zn precipitates in soil: A combined column-transport and XAFS study. *Environ. Sci. Technol.* **2002**, *36*, 3749−3754.

(7) Manceau, A.; Lanson, B.; Schlegel, M. L.; Harge, J. C.; Musso, M.; Eybert-Berard, L.; Hazemann, J.-L.; Chateigner, D.; Lamble, G. M. Quantitative Zn speciation in smelter-contaminated soils by EXAFS spectroscopy. *Am. J. Sci.* **2000**, *300*, 289−343.
(8) Juillot, F.; Morin, G.; Ildefonse, P.; Trainor, T. P.; Benedetti, M.; Laurence, G.; Calas, G.; Brown, G. E. Occurrence of Zn/Al hydrotalcite in smelter-impacted soils from northern France: Evidence from EXAFS spectroscopy and chemical extractions. *Am. Mineral.* **2003**, *88*, 509−526.
(9) Scheinost, A. C.; Kretzschmar, R.; Pfister, S.; Roberts, D. R. Combining selective sequential extractions, X-ray absorption spectroscopy, and principal component analysis for quantitative zinc speciation in soil. *Environ. Sci. Technol.* **2002**, *36*, 5021−5028.
(10) Manceau, A.; Marcus, M. A.; Tamura, N.; Proux, O.; Geoffroy, N.; Lanson, B. Natural speciation of Zn at the micrometer scale in a clay soil using X-ray fluorescence, absorption, and diffraction. *Geochim. Cosmochim. Acta* **2004**, *68*, 2467−2483.
(11) Manceau, A.; Tamura, N.; Celestre, R. S.; Macdowell, A. A.; Geoffroy, N.; Sposito, G.; Padmore, H. A. Molecular-scale speciation of Zn and Ni in soil ferromanganese nodules from loess soils of the Mississippi basin. *Environ. Sci. Technol.* **2003**, *37*, 75−80.
(12) Ressler, T. WinXAS: a program for X-ray absorption spectroscopy data analysis under MS Windows. *J. Synchrotron Rad.* **1998**, *5*, 118−122.
(13) Marcus, M. A.; Macdowell, A. A.; Celestre, R. S.; Manceau, A.; Miller, T.; Padmore, H. A.; Sublett, R. E. Beamline 10.3.2 at ALS: a hard X-ray microprobe for environmental and materials sciences. *J. Synchrotron Rad.* **2004**, *11*, 239−247.
(14) Decarreau, A. Cristallogenèse à basse température de smectites trioctaédriques par vieillissement de coprécipités silicométalliques de formule $(Si_{(4-x)}Al_x)M_3^{2+}O_{11}$, nH_2O, où × varie de 0 à 1 et où M^{2+} = Mg−Ni−Co−Zn−Fe−Cu−Mn. *Comptes Rendus l'Acad. Sci., Ser. II* **1981**, *292*, 61−64.
(15) Roberts, D. R.; Scheinost, A. C.; Sparks, D. L. Zinc speciation in a smelter-contaminated soil profile using bulk and microspectroscopic techniques. *Environ. Sci. Technol.* **2002**, *36*, 1742−1750.
(16) Manceau, A.; Lanson, B.; Drits, V. A. Structure of heavy metal sorbed birnessite. Part III: Results from powder and polarized extended X-ray absorption fine structure spectroscopy. *Geochim. Cosmochim. Acta* **2002**, *66*, 2639−2663.
(17) Sarret, G.; Saumitou-Laprade, P.; Bert, V.; Proux, O.; Hazemann, J.-L.; Traverse, A.; Martinez, C. E.; Manceau, A. Forms of zinc accumulated in the hyperaccumulator *Arabidopsis halleri*. *Plant Physiol.* **2002**, *130*, 1815−1826.
(18) Malinowski, E. R. *Factor analysis in chemistry*, 3rd ed.; Wiley-Interscience: New York, 2002.
(19) Ressler, T.; Wong, J.; Roos, J.; Smith, I. L. Quantitative speciation of Mn-bearing particulates emitted from autos burning (methylcyclopentadienyl)manganese tricarbonyl-added gasolines using XANES spectroscopy. *Environ. Sci. Technol.* **2000**, 34.
(20) Sarret, G.; Manceau, A.; Spadini, L.; Roux, J.-C.; Hazemann, J.-L.; Soldo, Y.; Eybert-Bérard, L.; Menthonnex, J.-J. Structural determination of Zn and Pb binding sites in *Penicillium chrysogenum* cell walls by EXAFS spectroscopy. *Environ. Sci. Technol.* **1998**, *32*, 1648−1655.
(21) Sarret, G.; Manceau, A.; Hazemann, J. L.; Gomez, A.; Mench, M. EXAFS study of the nature of zinc complexation sites in humic substances as a funtion of Zn concentration. *J. Phys. IV Fr.* **1997**, *7*, C2−799−802.
(22) Bochatay, L.; Persson, P. Metal ion coordination at the water−manganite (γ-MnOOH) inteface. II. An EXAFS study of zinc(II). *J. Colloid Interface Sci.* **2000**, *229*, 593−599.
(23) Roberts, D. R.; Ford, R. G.; Sparks, D. L. Kinetics and mechanisms of Zn complexation on metal oxides using EXAFS spectroscopy. *J. Colloid Interface Sci.* **2003**, *263*, 364−376.
(24) Manceau, A.; Chateigner, D.; Gates, W. Polarized EXAFS, distance-valence least-squares modeling (DVLS), and quantitative texture analysis approaches to the structural refinement of Garfield nontronite. *Phys. Chem. Miner.* **1998**, *25*, 347−365.
(25) Waychunas, G. A.; Fuller, C. C.; Davis, J. A. Surface complexation and precipitate geometry for aqueous Zn(II) sorption on ferrihydrite: I. X-ray absorption extended fine structure spectroscopy analysis. *Geochim. Cosmochim. Acta* **2002**, *66*, 1119−1137.
(26) Lindsay, W. L. *Chemical Equilibria in Soils*; John Wiley & Sons: New York, 1979.
(27) Helmke, P. A. In *Handbook of Soil Science*; Sumner, M. E., Ed.; CRC Press: Boca Raton, 1999; pp B/3−B/24.
(28) Scheffer, F.; Schachtschabel, P. *Lehrbuch der Bodenkunde, Scheffer/Schachtschabel*, 15th ed.; Spektrum Akademischer Verlag: Heidelberg, 2002.
(29) Johnson, C. A.; Glasser, F. P. Hydrotalcite-like minerals ($M_2Al(OH)_6(CO_3)_{0.5}XH_2O$, where M = Mg, Zn, Co, Ni) in the environment: Synthesis, characterization, and thermodynamic stability. *Clays Clay Miner.* **2003**, *51*, 357−357.
(30) Ford, R. G.; Scheinost, A. C.; Scheckel, K. G.; Sparks, D. L. The link between clay mineral weathering and the stabilization of Ni surface precipitates. *Environ. Sci. Technol.* **1999**, *33*, 3140−3144.
(31) Boclair, J. W.; Braterman, P. S. Layered double hydroxide stability. 1. Relative stabilities of layered double hydroxides and their simple counterparts. *Chem. Mater.* **1999**, *11*, 298−302.
(32) Allada, R. K.; Navrotsky, A.; Berbeco, H. T.; Casey, W. H. Thermochemistry and aqueous solubilities of hydrotalcite-like solids. *Science* **2002**, *296*, 721−723.

Received for review December 23, 2004. Revised manuscript received May 25, 2005. Accepted June 7, 2005.

ES047962G